Visual Neuroscience (1999), **16**, 637–652. Printed in the USA.

Receptive field and orientation scatter studied by tetrode recordings in cat area 17

P.A. HETHERINGTON AND N.V. SWINDALE

Department of Ophthalmology, University of British Columbia, Vancouver, British Columbia

(RECEIVED September 2, 1998; ACCEPTED January 20, 1999)

Abstract

The receptive-field positions and orientation preferences of neurons occupying the same tangential location in visual cortex are thought to be similar but to have an associated random scatter. However, previous estimates of this scatter may have been inflated by the use of subjective plotting methods, sequential recording of single units, and residual eye movements. Here we report measurements of receptive-field position and orientation scatter in cat area 17 made with tetrodes, which were able to simultaneously isolate and record up to 11 nearby neurons (ensembles). We studied 355 units at 72 sites with moving light and dark bars. Receptive-field sizes and positions were estimated by least-squares fitting of Gaussians to response profiles. We found that receptive-field position scatter was about half of the ensemble average receptive-field size. We confirmed previous estimates of orientation scatter, but calculations suggested that much of it may be accounted for by anatomical scatter in the positions of recorded neurons relative to the tetrode in a smooth map. Orientation tuning width was positively correlated with the degree of orientation scatter. Scatter was not independent in the two eyes: deviations from the local mean for both preferred orientation and receptive-field position were correlated although a significant amount of residual inter-ocular orientation and receptive-field position scatter was present. We conclude that cortical maps of orientation and receptive-field position are more ordered than was previously thought, and that random scatter in receptive-field positions makes a relatively small contribution to cortical point image size.

Keywords: Visual cortex, Orientation tuning, Disparity, Cortical maps, Multicellular recording

Introduction

Electrophysiological recordings in mammalian visual cortex have demonstrated that neurons located in columns of tissue running perpendicular to the surface have similar receptive-field properties and that these properties are mapped in a continuous and orderly fashion across the cortical surface (Hubel & Wiesel, 1962, 1968, 1974*a*,*b*). Area 17 in cats and monkeys contains an orderly topographic map of the visual field (Daniel & Whitteridge, 1961; Tusa et al., 1978), while orientation preferences change for the most part smoothly and periodically across the cortical surface (Hubel & Wiesel, 1962, 1974*b*; Albus, 1975*b*; Blasdel & Salama, 1986; Swindale et al., 1990; Bonhoeffer & Grinvald, 1991). A degree of randomness or scatter is believed to be superimposed on these smooth representations. Receptive field centers of sequentially recorded neurons have been found to be scattered in visual space over a region roughly equal to the size of the largest receptive fields in the recording sequence (Hubel & Wiesel, 1962, 1974*b*; Blakemore & Pettigrew, 1970; Creutzfeldt et al., 1974; Albus, 1975*a*). Scatter in the map of preferred orientation has also been observed, although estimates vary. Hubel and Wiesel (1968, 1974*a*) reported little or no scatter in the macaque monkey, but in the cat, preferences among neighboring cells have been reported to vary by as much as ±8 deg to ±23 deg (Albus, 1975*b*; Lee et al., 1977; Murphy & Sillito, 1986; Maldonado & Gray, 1996).

Scatter may be caused by random errors in cortical wiring, and degrade visual function, but it may subserve a positive functional role. For example, scatter in receptive-field center positions may increase the size of the "cortical point image"—the region of cortex containing neurons capable of responding to stimuli present at a single visual field location. Uncorrelated scatter in the receptive-field positions of the two eyes in binocularly driven neurons may confer cells with disparity selectivity and contribute to depth perception (Barlow et al., 1967; Nikara et al., 1968; Bishop, 1979), while uncorrelated scatter in orientation preferences may allow cells to detect slant in depth (Blakemore et al., 1972; Bishop, 1979; but see Nelson et al., 1977).

Before these possibilities can be assessed, however, it is necessary to be sure that scatter has been correctly estimated. Because scatter is, by definition, a measure of randomness, random measurement errors will lead to an overestimate of its magnitude. In fact several potentially significant sources of error are likely to have existed in previous studies. Measurements of receptive-field properties have usually been made sequentially (Hubel & Wiesel, 1962, 1974*b*; Albus, 1975*a*), but gradual drifts in eye position during recordings can produce random movements in field posi-

Correspondence and reprint requests to: N.V. Swindale, Department of Ophthalmology, University of British Columbia, 2550 Willow St., Vancouver, BC V5Z 3N9 Canada. E-mail: pah@ecc.ubc.ca

tions of several degrees (see also Rodieck et al., 1967; Chow & Lindsley, 1968; Bishop et al., 1971; Barlow et al., 1974; Albus, 1975*a*; Cynader et al., 1987). Although steps have usually been taken to correct for this problem (e.g. by measuring eye positions periodically, or by recording from a reference unit in the cortex or lateral geniculate nucleus), it is likely that the effects of eye movement have not been avoided entirely. A second source of error involves the common use of the "minimum response field" method (Barlow et al., 1967) to outline receptive-field borders and determine field positions. This method is subjective, tends to underestimate field sizes in weakly responsive cells (DeAngelis et al., 1995), and in some circumstances may cause neglect of the inhibitory regions of simple cell receptive fields. Neglecting these regions may also confound receptive-field positional differences with phase differences, which might also increase estimated positional scatter (Anzai et al., 1997).

We attempted to reduce these problems by making simultaneous recordings from groups of neurons with a tetrode, a group of four closely spaced metal microelectrodes (Gray et al., 1995) with which we were able to record simultaneously from ensembles of up to 11 nearby neurons in area 17 of the cat visual cortex. Our results suggest that receptive-field position scatter is much smaller than earlier reports suggested. Our estimate of orientation scatter is similar to previous reports, but we suggest that this amount might reasonably be expected in even a perfectly smooth orientation map because recorded neurons are likely to be randomly distributed over distances relative to the center of the tetrode which are significant on the scale of orientation column structure.

Materials and methods

Tetrode fabrication

Four, 15-cm strands of 25-μm (cats 1–3) or 12-μm (cats 4–12) nichrome wires (California Fine Wire, Grover Beach, CA) were wound together and coated with cyanoacrylate glue. The bundle was placed into a 6-cm-long, 30-μm (i.d.) insulated cannula, and affixed with Liquid Tape (GC Electronics, Rockford, IL). The wires protruded from the cannula approximately 1 cm on the recording end and 2 cm on the pre-amp end. The pre-amp ends were chemically stripped of insulation (Strip-X, GC Electronics), and attached to a 6-pin connector (Microtech, Inc., Boothwyn, PA). An additional grounding wire was attached to the cannula, and these five plus a sixth reference wire were bound together using Liquid Tape for protection and attached to the 6-pin connector. The tips of the tetrode wires were cut at an angle and gold plated to bring the electrode impedance to between 0.2 and 1.2 MΩ at 1 kHz. The tip separation varied from 15 μm to 35 μm, depending on the wire diameter and angle of cut.

Surgery and anesthesia

Twelve adult female cats were prepared for single-unit extracellular recording following guidelines established by the Canadian Council for Animal Care. Cats were initially sedated with oxymorphone (0.2 mg/kg, i.m.) and anesthetized with a bolus of sodium methohexital i.v., with continued i.v. injections to effect during the initial surgery. A tracheotomy was performed, and the animals were placed in a stereotaxic head holder and connected to temperature, BP, ECG, EEG, and end-tidal CO_2 monitors. Pressure points and wounds were infiltrated with a long-lasting local anesthetic (Marcaine, 0.25%) and dexamethasone (0.3 mg, i.m.) was given to prevent brain edema. A craniotomy approximately 5×5 mm in size was made with one edge close to the midline and extending from about -2 to -7 mm posterior to ear bar zero, over the crown of the lateral gyrus. The brain was viewed through a surgical microscope and a small area of dura was carefully removed. Methohexital injections were discontinued and light anesthesia maintained by artificially ventilating the animal with a mixture of 70% N_2O and 0.25–1.5% halothane or isoflurane in oxygen. Body temperature was maintained near 38°C with a thermostatically controlled heating pad, and end-tidal pCO_2 was monitored continuously and maintained near 40 mm Hg by varying the rate of an artificial respiration pump. Heart rate and EEG records were displayed on a computer monitor and recorded to disk. Paralysis was induced with pancuronium bromide and was maintained throughout the experiment by continuous i.v. infusion at a rate of 0.2 mg/kg/h together with oxymorphone at a rate of 0.01 mg/kg/h. These agents were dissolved in lactated Ringers, and delivered at a rate of 5 ml/kg/h. Pupils were dilated with topical atropine (5%) and nictitating membranes retracted with topical phenylephrine drops (10%). Contact lenses with 4-mm artificial pupils were selected on the basis of retinoscopic examination to focus the eyes on the display screen.

While viewing the exposed brain surface through a surgical microscope, we carefully placed the tetrode over a region free of blood vessels. To minimize dimpling of the cortical surface during tetrode penetration, we used a sharp electrode, bent at its tip into a tiny hook, to create a small tear in the *pia mater* immediately below the tetrode. The tetrode was then advanced into the cortex with a stepping motor microdrive. A blob of agar gel was placed in the craniotomy and allowed to set. The surface of the gel was coated with a viscous silicone oil to prevent drying.

Visual stimulation

Visual stimuli were generated by a computer controlled Picasso Image Synthesizer (Innisfree, Cambridge, MA) and displayed on a Tektronix 608 monitor with a maximum screen luminance of about 60 cd/m^2 and a minimum of about 9 cd/m^2. Initial rough estimates of the recorded neuron group receptive-field center and preferred orientation were made by hand plotting with a bright slit projected from a Welch Allyn ophthalmoscope. The display screen was then placed at the same location 40 cm (in a few cases 30 or 50 cm) distant from the eyes. Moving light or dark bar stimuli (typically 1–3 deg long and 0.15–0.4 deg wide) were programmed to make a series of sweeps across the aggregate receptive field at a variety of orientations (typically 5–11 conditions, 10–30 deg apart) and a variety of positions (typically 5–7 conditions, 0.5–1.0 deg apart) along an axis parallel to the axis of stimulus orientation. Stimulus ranges were chosen to include strongly responsive regions as well as flanking values producing weak or undetectable responses. The bar always moved at a constant velocity (typically 2–6 deg/s), chosen to match the velocity and direction preference of the units, perpendicular to the long axis of the bar. The width of the bar was chosen to be much narrower than the receptive-field width. The contrast of the bar (positive or negative), its orientation, and position were all randomly interleaved within a single complete set of stimuli, with each set repeated typically 8–16 times. There was a delay of approximately 200 ms between sweeps. Overall presentation times varied from 20–60 min. Stimuli were always viewed monocularly and usually both eyes were tested sequentially. Most receptive fields were 5–10 deg eccentric, near the vertical meridian, and in the contralateral, inferior visual field.

Physiological recording

Tetrode signals were passed from a unity gain amplifier located near the cat's head to a four-channel amplifier (model 1700, A-M Systems, Carlsborg, WA) (4k–10k gain, 300 Hz to 5 kHz band pass) and then to an audio monitor and a four-channel oscilloscope. For on- and off-line analysis, the voltage waveforms were digitized by a 12-bit, 32-kHz (per channel) A/D board (Data Translation DT2821, Marlboro, MA). If a spike with an amplitude greater than three times noise (typically 20–30 μV) was detected on any of the four channels, a data record from all four channels was stored on disk (Discovery V5.1, DataWave Technologies, Thornton, CO). In addition, 12-bit values proportional to bar length, width, horizontal and vertical position, contrast, and orientation were also stored to disk at a rate of 60 Hz, together with a time stamp accurate to 0.1 ms.

Multiunit spike separation

Whenever a spike was detected, peak and valley waveform voltages from each of the four tetrode channels were extracted. These eight parameters were converted into standard scores (z-scores) and displayed in various [$N(N-1)/2 = 28$ possible] two-dimensional projections (e.g. peak on channel 1 *vs*. peak on channel 3) as points on a computer screen (Fig. 1). Individual units were usually visually identifiable as clusters in one or more of such plots. Because variability in the eight parameter values is not independent, and may be influenced by factors such as firing rate and correlated noise, the clusters tend to be elliptical in shape, so ellipses were used to define and separate the clusters of each of the units recorded (Hetherington et al., 1996). A computer program (written by P.A. Hetherington; Autocut V3.0, DataWave Technologies) was used to define the ellipses in the following way. All 28 projections were viewed simultaneously on screen and projections which showed clear separations between clusters were selected. In each of these projections one or more elliptical borders were drawn under visual control until each cluster had been outlined. From the statistics (means, variances, and covariances) of the points contained within the elliptical border, ellipses were computed for all projections. These ellipses were later manually adjusted to best match the cluster shapes and were then used to separate the clusters in a cookie cutter fashion. The multidimensional elliptical borders were computed from a sample (e.g. 3000 spikes) of the total number of spikes collected, and were then used to classify the rest of the spikes in the data file. Any point which fell within the elliptical boundaries of two or more clusters was assigned to the most probable cluster (Hetherington et al., 1996). Suspected shifts of the electrode relative to tissue during the experiment and consequent slow drifts in signal amplitudes were automatically corrected for during spike separation by adaptively moving the cluster boundaries relative to the slow movement of the cluster centers with time. If these drifts proved too large and/or cluster boundaries could not confidently be assigned, the data from the cluster were rejected.

Receptive field and orientation tuning

Preferred orientation and receptive-field positions and sizes were estimated by least-squares fitting of a Gaussian or Gabor function using a simplex algorithm (Nelder & Mead, 1965). Preferred orientation was first estimated from the center of a wrapped Gaussian (Batschelet, 1981; Swindale, 1998) fit to the profile of responses summed across all other stimulus conditions. Using only the orientation stimulus condition that corresponded most closely to this estimated preferred orientation, a Gaussian was fit to the receptive-field length profile and its center estimated. From the sweep that was closest to the length profile center (or from both sweeps if the center lay closer to the boundary between two adjacent bins than to one of the two bin centers), the final preferred orientation was computed. From this final preferred orientation, the length center was recomputed as above to yield a final preferred length center and size. And from the preferred orientation and preferred length center, the receptive-field width profile was obtained for both the light and dark bar responses.

Before a function could be fit to the width profiles, the cell had to be defined as either simple or complex. To accomplish this algorithmically, a normalized spatial correlation between the light and dark bar responses was obtained (Swindale & Mitchell, 1994),

$$C/S = \frac{\sum_i R_i^+ R_i^-}{\sqrt{\sum_i (R_i^{+2}) \times \sum_i (R_i^{-2})}}, \quad (1)$$

where R_i^+ and R_i^- are the firing rates at a sweep position i to light and dark bars, respectively. This formula yields a number from 0 to 1, where 0 means that the light and dark bar responses are spatially uncorrelated, and 1 means that the two are perfectly correlated. Following Swindale and Mitchell, we defined cells with $C/S > 0.5$ as complex, and those with $C/S \leq 0.5$ as simple. For simple cells, the dark bar response was subtracted from the light bar response and a Gabor function (Marcelja, 1980; Jones & Palmer, 1987) was fit to the profile. For complex cells, light bar and dark bar responses were added and a Gaussian fitted.

The center and size of the Gaussian (complex cell) or the Gaussian envelope of the Gabor function (simple cell) provided an estimate of the center and size of the cell's receptive-field width. Although in theory a Gaussian has no edges, for the purposes of measurement we define the edges to be at $\pm 2\sigma$ from the center. This corresponds to the points where lines drawn tangent to the inflection points (at $\pm 1\sigma$) intersect the x axis, and bracket the 95% confidence intervals. Receptive-field size was defined as the square root of the product (geometric mean) of the receptive-field length and width.

Measures of scatter

The standard deviation (unbiased estimate) of cell positions or orientations around the mean in each ensemble was calculated and used as an estimate of variability in receptive-field center position or orientation preference in each ensemble. An unbiased estimate of overall or mean group scatter across all ensembles, σ, was calculated according to the following formula (Barlow, 1989):

$$\sigma = \sqrt{\frac{\sum_{i=1}^{ngrps} \left(\sum_{j}^{ncells} (X_j - M_i)^2 \right)}{\sum_{i=1}^{ngrps} (n_i - 1)}}, \quad (2)$$

where X_j is the receptive-field position of cell j, M_i is the mean of the positions in each group, and n_i is the number of cells in each group. In most situations, we took 4σ to provide a more intuitive estimate of the range of variation ($\pm 2\sigma$).

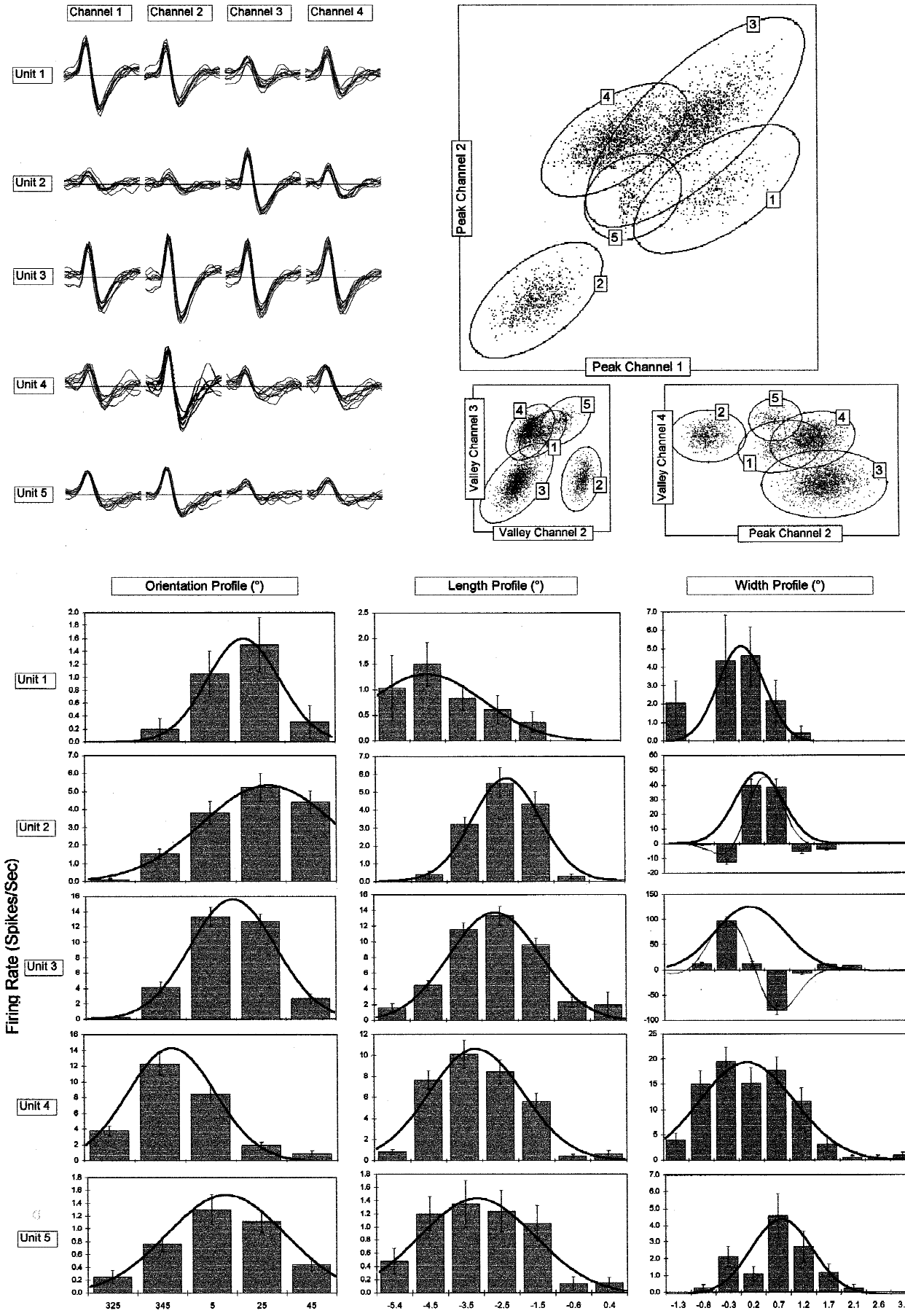
Channel 1
Channel 2
Channel 3
Channel 4
Unit 1
Unit 2
Unit 3
Unit 4
Unit 5
Peak Channel 2
Peak Channel 1
Valley Channel 3
Valley Channel 2
Valley Channel 4
Peak Channel 2
Orientation Profile (°)
Length Profile (°)
Width Profile (°)
Firing Rate (Spikes/Sec)
325 345 5 25 45
-5.4 -4.5 -3.5 -2.5 -1.5 -0.6 0.4
-1.3 -0.8 -0.3 0.2 0.7 1.2 1.7 2.1 2.6 3.1

FIGURE 1

To allow comparisons between our measures of scatter and those obtained in previous studies, which have used more than one definition, we calculated the mean, or sometimes the median, cell pair difference in receptive-field center position or orientation taken across all cell pairs in each ensemble, over a set of ensembles. This is the average (or median) difference in receptive-field centers between two neighboring visual cortical cells. Note that while the cell pair difference measure is an intuitive estimate of scatter, and has been used in previous papers, histograms of cell pair differences taken from a normal distribution will be skewed, and the mean of the pair differences overestimates the true standard deviation of radial distances from the mean by about 25%. Because the histograms of absolute cell pair differences were skewed, for any statistics involving these numbers, a closer approximation to the normal distribution was obtained by taking the square root of each value (Tabachnick & Fidell, 1989). In no case did transforming a distribution in this way change the interpretation of the results.

For orientation data, means and variances were calculated using circular statistics (Batschelet, 1981; Fisher, 1995). Correlations between two uniformly distributed circular variables were computed using Batschelet's circular–circular correlation and for normal distributions Fisher's (1995) circular–circular correlation was used. For correlations between linear and circular variables (e.g. receptive field *vs*. orientation scatter), Fisher's linear–circular correlation was used. All other noncircular correlations were computed using the common Pearson's *r* correlation coefficient.

In the scatter plots of such variables as receptive field and orientation scatter, we sought to determine the best-fit lines that would allow the prediction of one variable from the other. However, when both variables are dependent measures, linear regression cannot be used because it assumes errors on only the *y*-axis variable. Instead, we used a maximum likelihood regression technique which fits straight lines to data with errors in both dimensions (Barlow, 1989). The best straight line fit is given by $Y = mX + b$, where

$$m = A \pm \sqrt{A^2 + 1}, \qquad \text{and} \qquad A = \frac{Var_y - Var_x}{2 \times Cov_{x,y}}. \tag{3}$$

Var is the variance of *x* or *y*, and $Cov_{x,y}$ is the covariance of *x* and *y*. The two values of *m* resulting from the ± sign correspond to the first and second principal components of the data, respectively. If $Cov_{x,y}$ is positive, then the ± sign is taken as positive, otherwise it is negative. On each scatter plot, we draw this best-fit line and report its prediction equation.

Results

Number of cells

Recordings were made from cell ensembles at a total of 72 sites in 12 cats. Fig. 2 shows the distribution of the number of cells per ensemble at monocularly and binocularly (first one eye then the other) recorded sites. The number of cells in each ensemble varied between two and 11 (mean = 4.9 ± 1.8) yielding a total of 355 cells in all. Of these, 256 (72%) demonstrated both good orientation and receptive-field tuning in at least one eye. Neglecting ensembles of less than three cells, and taking all cell pairings in each ensemble, this allowed for an analysis of 478 cell pairs from 53 ensembles (in cases when data were available for both eyes, the eye with the largest number of responding cells in the ensemble was chosen for analysis). Binocular data were obtained from a total of 138 cells at 24 sites in seven cats, of which 94 (68%) demonstrated good orientation and receptive-field tuning in both eyes. The number of cells recorded at each site was similar to that reported by other investigators using tetrodes in visual cortex (e.g. Gray et al., 1995; Maldonado & Gray, 1996).

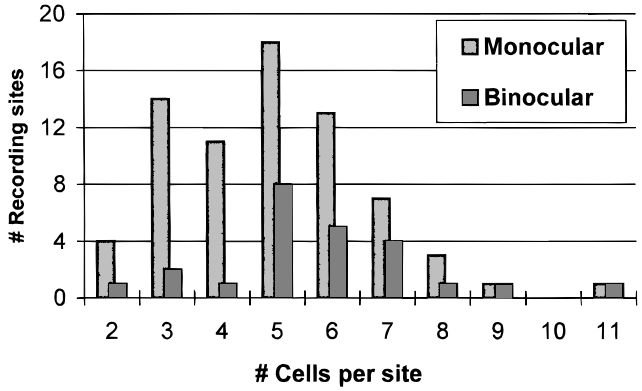

Fig. 2. The distribution of ensemble sizes (cells per recording site). Sites from which binocular data were obtained are indicated separately.

Laminar distribution

All penetrations were made nearly perpendicular to cortical surface, at or near the crown of the lateral gyrus, and the distance from the cortical surface was recorded at each site. Most (90.3%) of the cells were obtained at depths from 100 μm to 900 μm. To determine if the depth of recording accounted for any significant amount of variance in receptive-field size or scatter, or orientation tuning width and scatter, the depths were binned into upper (1–300 μm), middle (301–600 μm), and lower (601–900 μm) thirds.

The only property found to vary significantly with depth was receptive-field size. Receptive fields were larger in the upper and lower thirds than in the middle third [$F(2,333) = 9.13$, $P < 0.0001$]. Receptive-field scatter, orientation tuning width, and orientation scatter did not vary significantly with cortical depth. To simplify our analysis of receptive field and orientation scatter, and

Fig. 1. The top left-hand panel shows voltage waveforms from five simultaneously recorded units (labeled 1–5) on the four channels of the tetrode. Note the consistency of spike shape and that each of the five units gives rise to a distinct set of waveforms on the four channels. The three panels on top right show selected pairs of the eight waveform parameters (peak-and-valley voltages on four channels) plotted against each other, with each dot representing a single spike. Note that the dots fall into distinct clusters, and that clusters are more distinct in some projections than others (e.g. the clusters labeled 3 and 5 are not distinct in the top projection but are clearly separated in the two lower projections). The bottom half of the figure shows tuning profiles for orientation, receptive-field length and width, for each of the five units. The solid lines are the best-fit Gaussian functions, and the thin lines are best-fitting Gabor functions to simple cell receptive-field width profiles.

because neither receptive field nor orientation scatter varied with depth, all further analyses of scatter were collapsed across cortical depth.

Receptive-field scatter

Receptive fields were obtained at an eccentricity of 5–10 deg from the fovea, in the contralateral, inferior visual field near the vertical meridian. The mean group scatter in field positions across all ensembles of more than three cells was 0.48 deg ($4\sigma = 1.94$ deg, $N = 53$). The mean absolute difference in receptive-field center position between neighboring cell pairs was 0.82 deg ± 0.59 deg ($N = 478$). As expected, the distribution of differences was positively skewed (see Fig. 7B, "Experimental Data"), and the median (0.68 deg) rather than the average provided a better estimate of the cell pair difference.

To compare receptive-field position scatter with receptive-field size, we compared the receptive-field position standard deviation for each site at which three or more cells were recorded ($N = 53$) against mean group receptive-field size (Fig. 3A). There was a small, but significant correlation between receptive-field size and scatter in receptive-field position ($r = 0.33$, $P < 0.02$). The average receptive-field size (4σ) of all cells recorded ($N = 256$) was 3.80 deg ± 1.83 deg, whereas the mean scatter (4σ) was only 1.94 deg. Although receptive-field scatter increased as the receptive-field size increased, the amount of scatter was far less than that expected from receptive-field size. In fact, in only two of the 53 groups recorded was scatter greater than the aggregate field size. The average ratio of receptive-field scatter to receptive-field size was 0.45.

An analysis of cell pair differences showed a similar result. The difference in receptive-field position for all 478 cell pairs was plotted against the mean receptive-field size (4σ) in Fig. 3B. The cell pair difference in receptive-field position was weakly but significantly correlated with the mean of the cell pair receptive-field size ($r = 0.22$, $P < 0.001$) although because only a small range of visual field eccentricities was sampled, a strong correlation was not expected. It is clear, however, that estimates of scatter were always substantially smaller than receptive-field size. The average ratio of cell pair receptive-field difference to cell pair mean receptive-field size was 0.25.

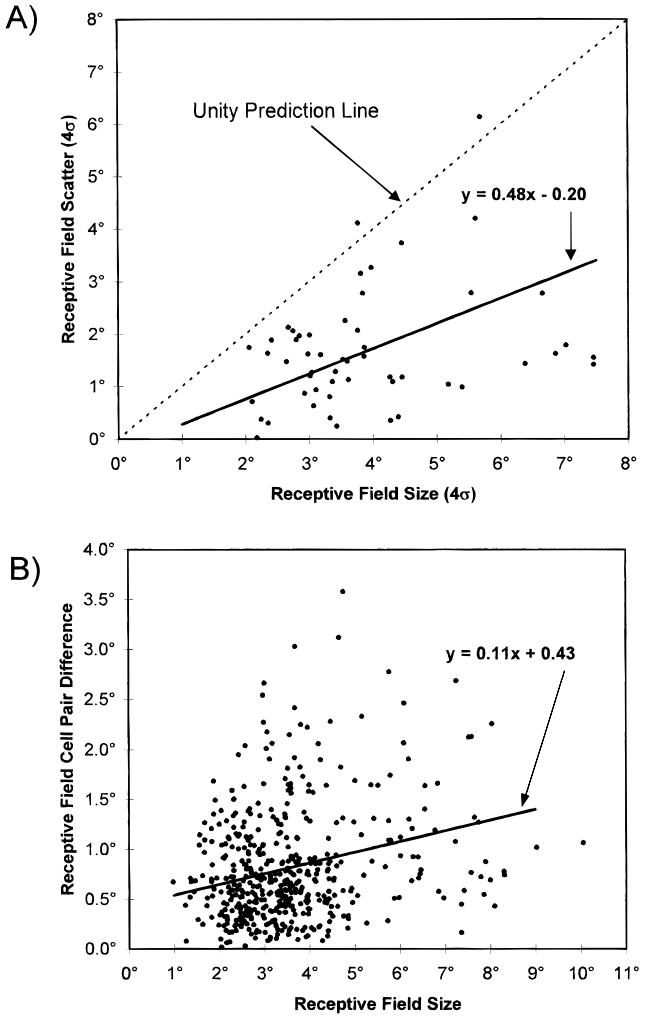

Fig. 3. (A) Scatter plot showing the mean receptive-field size of each cell ensemble on the *x* axis, and the scatter of receptive-field center positions within each ensemble on the *y* axis. Note that, on average, scatter is just less than half of the mean receptive-field size. (B) Scatter plot showing the mean receptive-field size of each simultaneously recorded cell pair on the *x* axis and the distances between the receptive-field centers of each pair on the *y* axis.

Horizontal vs. vertical scatter

We found no evidence for any difference in the horizontal and vertical components of receptive-field position scatter. On the basis of *t*-tests, the mean absolute cell pair horizontal receptive-field difference (0.51 deg ± 0.49 deg, median = 0.37 deg) did not differ significantly from the mean absolute cell pair vertical difference (0.53 deg ± 0.47 deg, median = 0.41 deg). Similarly, horizontal standard deviations (4σ = 1.81 deg ± 1.33 deg, median = 1.43 deg, mean group horizontal scatter = 2.10 deg) did not differ significantly from vertical standard deviations (4σ = 1.89 deg ± 1.23 deg, median = 1.63 deg, mean group horizontal scatter = 2.12 deg).

Ipsilateral eye vs. contralateral eye receptive-field scatter and disparity

In binocular ensembles we found no significant difference in absolute individual receptive-field deviations (deviations × 4) between ipsilateral (I) and contralateral (C) eyes (I = 1.18 deg ± 0.88 deg, C = 1.02 deg ± 0.89 deg), nor in the amount of vertical (I = 1.60 deg ± 1.21 deg, C = 1.76 deg ± 1.66 deg), horizontal (I = 1.65 deg ± 0.70 deg, C = 1.67 deg ± 1.12 deg), or combined (i.e. radial) (I = 1.56 deg ± 0.68 deg, C = 1.66 deg ± 1.04 deg) group standard deviation. The ipsilateral eye scatter (4σ) was 1.75 deg, while the contralateral eye scatter was 1.79 deg.

Individual deviations

Within binocular ensembles, ipsilateral eye deviations of individual unit receptive-field positions from the ensemble mean were significantly correlated with contralateral eye deviations from the mean (Figs. 4 and 5) ($r = 0.41$, $P < 0.001$, $N = 85$). Thus, receptive fields which were to the upper left of the group center in one eye were also to the upper left of the center in the other eye. This relationship was due more to correlations between vertical than horizontal deviations. The correlation across the eyes was greater for vertical deviations ($r = 0.55$, $P < 0.001$) than for

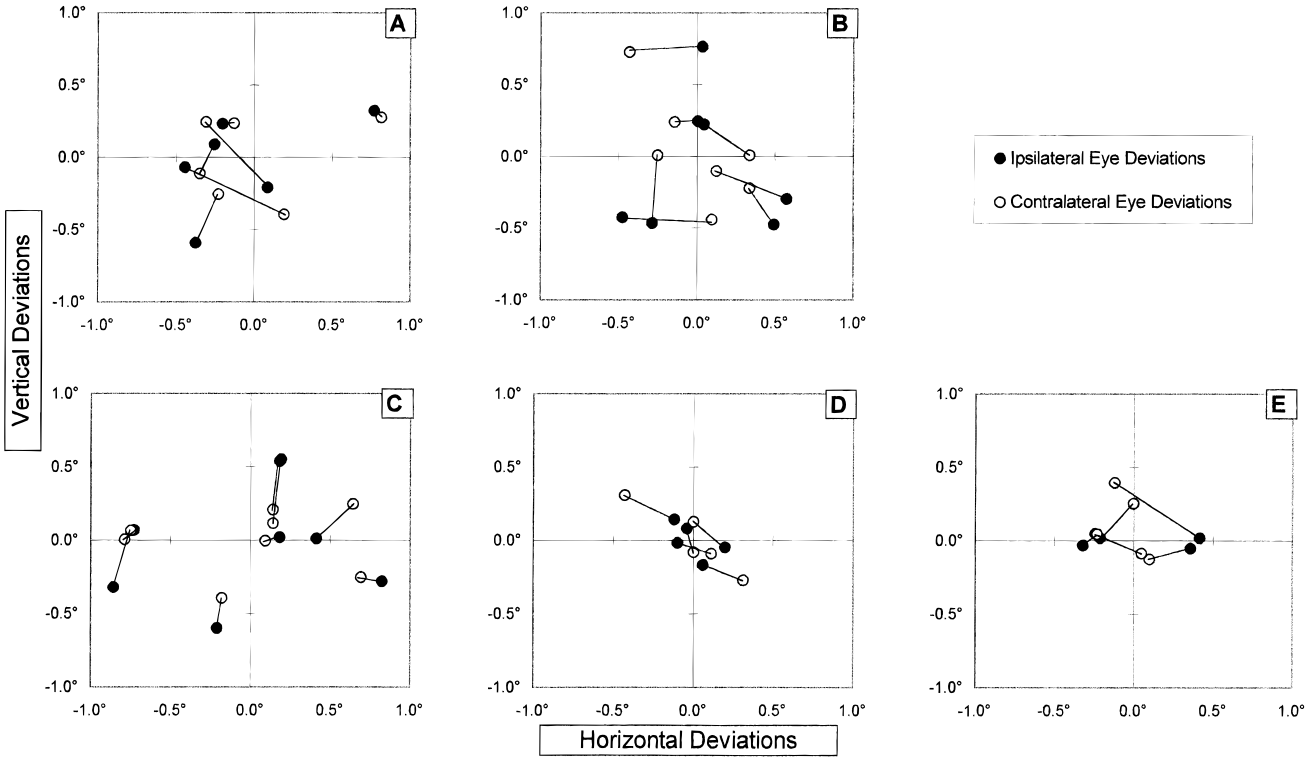

Fig. 4. Graphs from five ensembles (A–E) from which binocular data were obtained. The *x* axes show the horizontal deviation of each receptive-field center relative to the mean horizontal receptive-field position in each ensemble, and the *y* axis similarly shows the vertical deviation relative to the mean. Ipsilateral and contralateral eye data points from the same cell are connected by lines. Note that ipsilateral eye and contralateral eye deviations are correlated.

horizontal deviations ($r = 0.23$, $P < 0.05$; vertical *r vs.* horizontal *r*: $P < 0.001$, although see below).

Receptive-field scatter was also correlated across the eyes ($r = 0.62$, $P < 0.01$, $N = 18$) (Fig. 6A). Thus, ensembles with a high degree of scatter in one eye tended to have a high degree of scatter in the other eye. And, as above, this relationship was mainly due to correlations between vertical and not horizontal components of scatter. The amount of vertical scatter was correlated across the eyes (Fig. 6B, $r = 0.67$, $P < 0.01$), but the amount of horizontal scatter was not (Fig. 6C, $r = -0.12$, P = NS; vertical *r vs.* horizontal *r*: $P < 0.001$).

The low correlation between the horizontal deviations (individual and group) across the eyes means that horizontal disparities were greater than vertical disparities. Statistically, the average horizontal receptive-field disparity (0.34 deg ± 0.35 deg) was significantly greater than average vertical receptive-field disparity (0.25 deg ± 0.24 deg, $t(84) = 2.00$, $P < 0.05$). However, this statistical difference was not robust: it was partially dependent on the inclusion of two outliers ($> 4\sigma$ from the mean), seen in the top left and bottom right of Fig. 5A. With these two outliers excluded, individual horizontal deviations were correlated across the eyes ($r = 0.43$, $P < 0.001$) and this correlation was not significantly different from the correlation between individual vertical deviations. The correlation between horizontal scatter remained unchanged, but the difference between horizontal (0.30 deg ± 0.24 deg) and vertical (0.25 deg ± 0.24 deg) disparities failed to reach significance ($P = 0.078$). Thus, our data suggest that if there is a difference between horizontal and vertical receptive-field position disparities, it is likely to be small.

Simple vs. complex cells

The average receptive-field scatters (4σ) and sizes (4σ) of simple and complex cells ($N = 85$) are presented in Table 1. Simple cells had significantly greater overall, vertical, and horizontal scatter than did complex cells, in spite of their slightly smaller overall size. Note that because the receptive-field centers of simple cells were obtained from Gaussian envelops of fit Gabor functions, it is unlikely that phase differences could account for the larger scatter among simple cells (cf. Anzai et al., 1997).

Orientation scatter

The average cell pair ($N = 478$) difference in orientation preference (Fig. 7A) was 15.4 deg ± 17.0 deg (median = 9.42 deg). The average of the maximum cell pair difference across groups was 28.6 deg ± 21.5 deg, and the largest cell pair difference in any group was 89.7 deg. The mean group scatter ($N = 53$) was 13.65 deg (median $\sigma = 8.4$ deg, max. $\sigma = 33.8$ deg).

As expected, orientation preferences in the two eyes were highly correlated ($r = 0.93$, $P < 0.001$), and there was a consistent right minus left eye difference in preference averaging 13.5 deg ± 8.2 deg across all animals, likely resulting from constant intorsion of the eyes caused by paralysis (Nelson et al., 1977; Cooper & Pettigrew, 1979). Orientation scatter in ipsilateral and contralateral eyes (Fig. 8A) was positively correlated ($r = 0.68$, $P < 0.01$, $N = 18$); that is, ensembles with a large orientation scatter in one eye tended to have a large scatter in the other eye. Consistent with this, deviations in preferred orientation, relative to the group mean

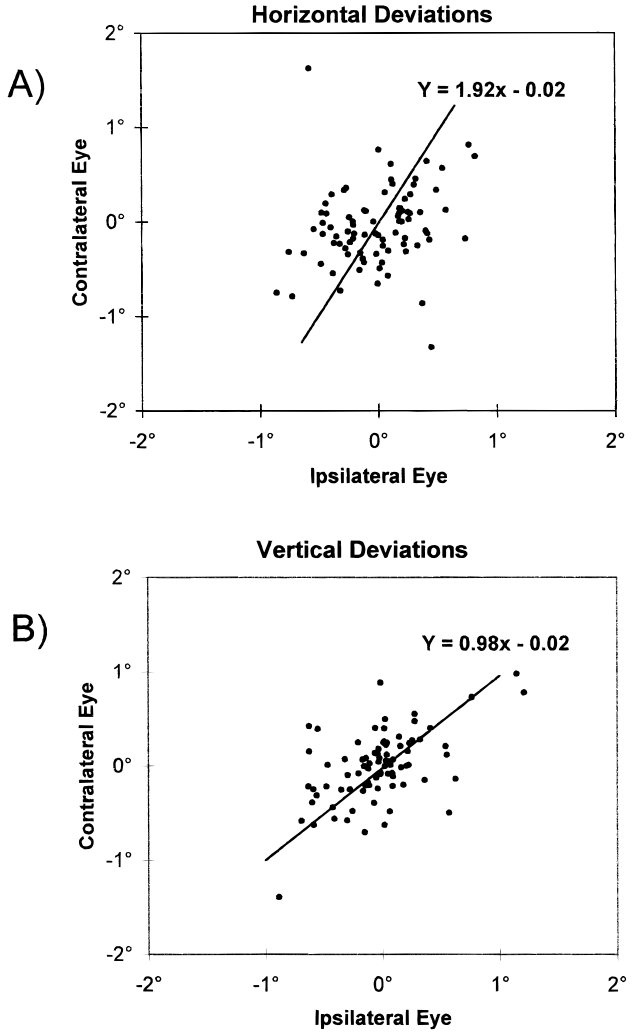

Fig. 5. Scatter graphs showing the correlation between (A) the horizontal deviations from the group means for contralateral eye *versus* ipsilateral eye receptive-field position centers; (B) the vertical deviations from the group means. If the two outliers in (A) are removed, no statistical difference occurs between the two correlations reported in Results.

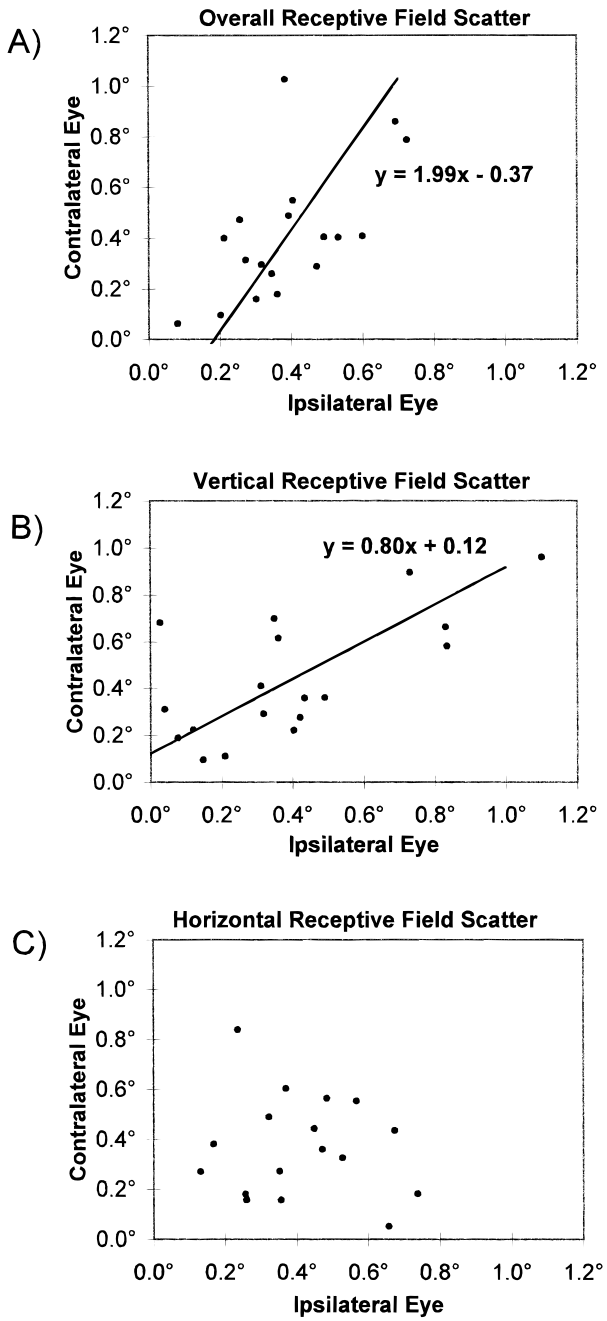

Fig. 6. Graphs of contralateral eye *versus* ipsilateral eye receptive-field scatter, measured as the standard deviation of receptive-field center position relative to the ensemble mean. (A) Overall scatter (i.e. radial component of receptive field position); (B) vertical component of scatter; and (C) horizontal component of scatter.

in each ensemble (Fig. 8B), were significantly correlated across eyes ($r = 0.41$, $P < 0.001$, $N = 85$). There was no significant difference between the ipsilateral and contralateral eyes in the absolute amount of orientation scatter, nor was there any significant difference in scatter between simple (12.0 deg) and complex (11.8 deg) cells.

The relationship between orientation scatter and orientation tuning width was similar to that found between receptive-field position scatter and receptive-field width. Orientation scatter of all groups including three or more cells was compared with the mean group orientation tunings. Fig. 9 shows that orientation scatter was strongly correlated with orientation tuning width ($r = 0.70$, $R^2 = 0.49$, $P < 0.001$, $N = 53$). Just as group receptive-field scatter was almost always less than group receptive-field size, group orientation scatter was also always less than group orientation tuning, with the average ratio of orientation scatter to orientation tuning equal to 0.32.

Receptive-field scatter vs. orientation scatter

Scatter of receptive-field position and orientation preference was not significantly correlated across ensembles (Fig. 10A) ($r = 0.01$, $P =$ NS, $N = 53$), that is, ensembles showing a large amount of scatter in receptive-field position did not show a correspondingly large scatter in preferred orientation. Nor were the individual deviations of orientation and receptive-field position from the local

Table 1. *Differences in receptive field scatter and size between simple and complex cells*

	Simple (deg)	Complex (deg)	*P* value (2-tailed)
Receptive-field scatter			
Overall	1.92	1.63	0.042
Vertical	2.32	1.63	0.0005
Horizontal	2.36	1.47	0.021
Receptive-field size			
Overall	3.62	4.03	0.056 (1-tailed)
RF Length	6.01	5.10	0.032
RF Width	2.42	3.31	0.0003

mean correlated ($r = 0.07$, P = NS, $N = 256$). The absolute values of cell pair receptive-field position and orientation differences did however show a small significant positive correlation (Fig. 10B) ($r = 0.19$, $P < 0.001$, $N = 478$). A possible explanation of this result is that the cortical distances between simultaneously recorded cell pairs vary: cell pairs which are further apart will on average have slightly greater absolute differences in receptive-field positions and orientation preferences than cell pairs close together. If true, this implies that anatomical scatter in the positions of recorded cells relative to the tetrode is significant, and that local order in the cortical map has a detectable impact on the variation in receptive-field properties within simultaneously recorded ensembles. Evidence relevant to this possibility is examined in more detail in the following section.

Estimation of expected scatter in smooth orientation and retinotopic maps

Orientation preference varies relatively rapidly over the surface of area 17, undergoing a 180 deg rotation on average about every 1.1 mm (Löwel et al., 1987; Diao et al., 1990). This raises the possibility that some of the observed orientation scatter in cell ensembles might be caused by tangential positional scatter of the cells recorded by the tetrode. It has been shown that cortical microelectrodes can record from cells which are 50–100 μm distant from the electrode tip (see Mountcastle et al., 1957; Humphrey et al., 1978; Drake et al., 1988); and it is estimated that tetrodes, which are typically 30–80 μm in diameter, can record from cells within distances up to about 65 μm from the center of the tetrode (Gray et al., 1995; Maldonado & Gray, 1996). This means that some cell pairs might be up to 130 μm apart. Assuming an average orientation gradient of 180 deg per 1.1 mm, this translates to a maximum orientation difference of 21 deg, which does not seem inconsistent with the data (Fig. 7). A more exact estimate of the distribution of cell pair orientation differences requires a knowledge of the variation in the spatial rates of change of orientation preference, and of the distribution of recorded cells relative to the tetrode. Orientation gradient is high close to singularities and lower elsewhere (Blasdel & Salama, 1986; Bonhoeffer & Grinvald, 1991) and the overall pattern of preference can be described reasonably well by simple models (reviewed in Swindale, 1996). The likely distribution of recorded cells relative to the tetrode is difficult to assess. We tested two simple models, one in which recorded cells were assumed to be distributed uniformly in a circle of radius 65 μm (model A), and another in which cells were assumed to be uniformly distributed within a circle equal to the diameter of the tetrode (about 60 μm) with an additional lateral Gaussian scatter of ± 60 μm (model B). We used a computer-generated orientation map (Swindale, 1982) which had a singularity density of 2.2 per 1.1 mm^2, similar to that observed experimentally (Wolf & Geisel, 1998), and a resolution of 1 pixel = 5 μm. At each of 5000 randomly positioned sites, a set of eight surrounding cell positions was calculated according to the assumed distribution. The frequency histogram of the differences in orientation between pairs of cell positions in the map was calculated (Fig. 7A). Model A gave an imprecise fit to the data although it was able to account for a substantial amount of scatter. The fit with model B was better, although the experimental distribution is somewhat flatter near the origin, and may have slightly more cases with large orientation differences. As would be expected, the singularity density had an impact on the amount of scatter: when the calculations were repeated on an orientation map with the same periodicity, but with parallel iso-orientation domains lacking singularities, the amount of scatter (measured as the 2nd moment of the distribution) decreased from 10.7 deg to 7.5 deg (model A) and from 18.3 deg to 14.2 deg (model B). Given the uncertainties in the actual sampling distribution of the tetrodes, these calculations are not conclusive, but they raise the possibility that a large component of experimentally measured orientation scatter might be attributable to anatomical scatter in the positions of recorded cells relative to the tetrode.

Could the observed scatter in receptive-field position be accounted for in the same way? Assuming an entirely smooth and uniform cortical map, anatomical scatter of cell positions can be translated into scatter in retinal coordinates if cortical magnification factor is known. At an eccentricity of 5–10 deg from the fovea, in the contralateral, inferior visual field near the vertical meridian, where the present recordings were made, cortical magnification factor is about 2 deg/mm (Albus, 1975*a*). When the preceding calculations were repeated, the resulting cell pair position differences were much smaller than the experimentally observed ones for all reasonable parameter values (Fig. 7B). A good agreement between the simulation and experiment could only be obtained by the improbable assumption of a tetrode seeing distance of ± 180 μm. This suggests that positional scatter of recorded cells relative to the tetrode contributes relatively little to the observed scatter in receptive-field position.

Receptive field and orientation scatter vs. estimated cortical distance

Although it might be possible in principle, we have not attempted to reconstruct the positions in the cortex of recorded cells relative to each other and to the tetrode. However, it is relatively easy to compute a measure which is likely to correspond approximately to the physical distances between simultaneously recorded cell pairs. Two cells whose spikes yield similar peak-and-valley voltages on all four channels are likely to be physically closer than cells with peak-and-valley voltages that are dissimilar. The degree of similarity can be calculated by representing each cell as a point in an eight-dimensional space, the axes of which represent the standardized scores of the four peak voltages and four valley voltages. The Euclidean distances between points in this space, which we refer to as a *z*-score distance, can be assumed to vary, at least in part, with the physical

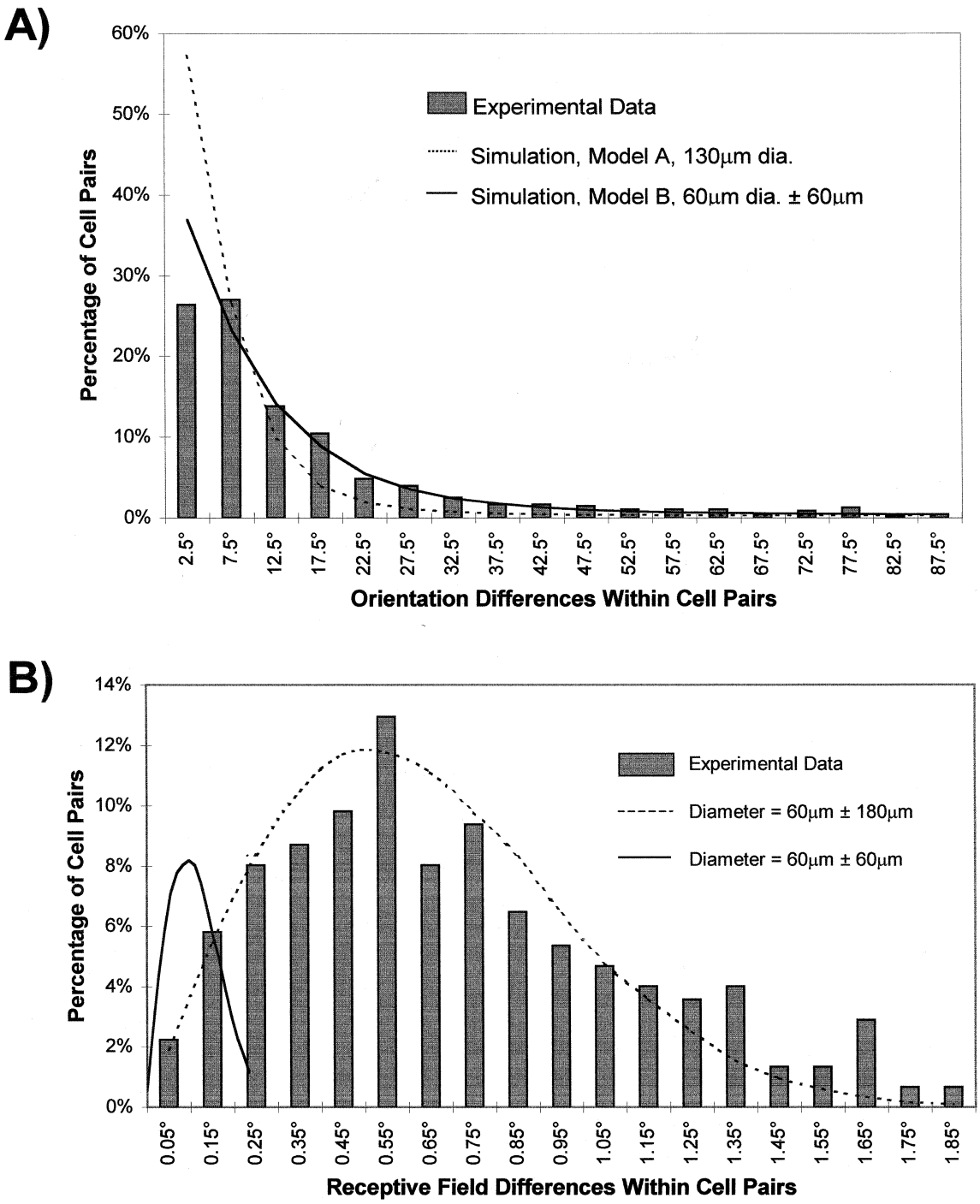

Fig. 7. (A) Histogram of the difference in preferred orientation of simultaneously recorded cell pairs (gray bars). Dashed and solid lines show the predicted distribution of orientation differences for models A and B, respectively, described in more detail in the Results section. These models assume a locally smooth orientation map together with a degree of random scatter in the positions of recorded cells relative to the center of the tetrode. (B) Histogram of the distances between the receptive-field centers between members of simultaneously recorded cell pairs. Lines show the predicted distribution of distances assuming a cortical magnification factor of 2 deg/mm, no physiological scatter, and random scatter in the positions of recorded cells relative to the center of the tetrode. The solid line shows the amount of scatter predicted by model B which is able to explain nearly all of the observed orientation scatter. The dashed line shows that the observed receptive-field position scatter can only be explained in anatomical terms by assuming an implausibly large amount of scatter in recorded cell positions (± 180 μm), implying that most of the observed scatter is physiological in origin.

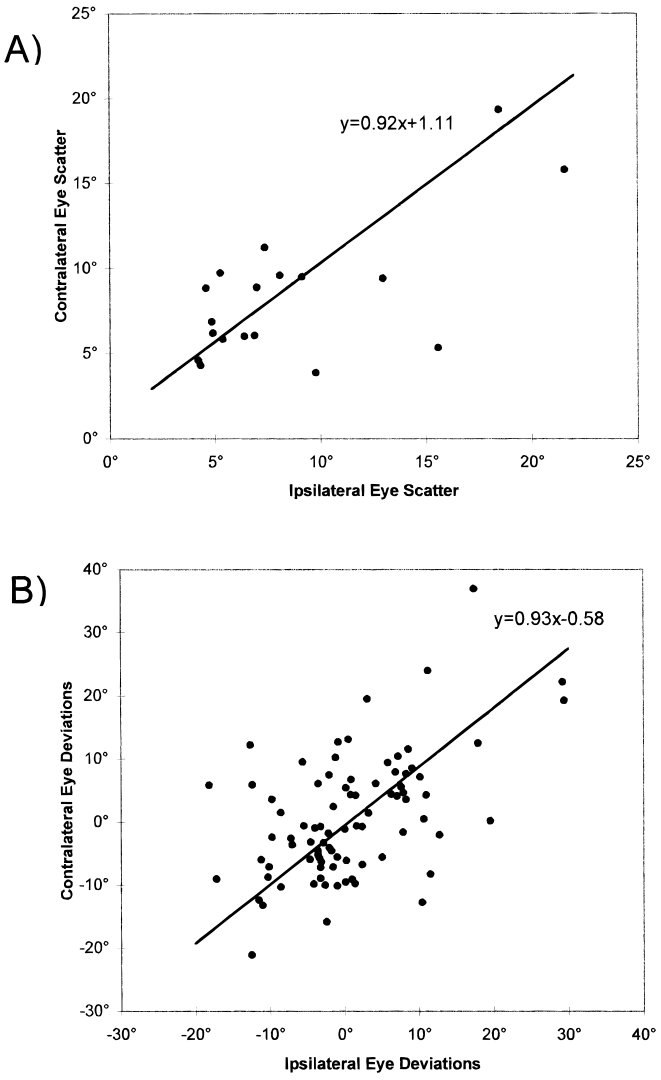

Fig. 8. (A) Scatter plot showing orientation scatter in contralateral *versus* ipsilateral eyes: ensembles showing a large orientation scatter in one eye were likely to show a large scatter in the other eye. (B) Scatter plot showing, for each binocularly studied cell in ensembles of three or more cells, the deviation in preferred orientation relative to the ensemble mean in the contralateral eye *versus* the ipsilateral eye.

distance between the cells: two nearby cells can be expected to have a small *z*-score distance, while two relatively distant cells can be expected to have a large *z*-score distance. If our arguments about the impact of cell position scatter on receptive-field properties are correct, then the average *z*-score distance between the spikes of two cells should vary with both their receptive-field position difference and their preferred orientation difference.

The results support the hypothesis, but for receptive-field position differences only. As the estimated cortical distance between neighboring cells increased, so, on average, did the vertical ($r = 0.15$, $P < 0.01$), horizontal ($r = 0.10$, $P < 0.05$), and combined ($r = 0.16$, $P < 0.001$) receptive-field position differences ($N = 478$). Surprisingly, we found no significant correlation ($r = -0.02$) between the difference in preferred orientation and estimated cortical distance.

Discussion

Receptive-field scatter

The estimated scatter of receptive-field center positions in our sample of ensembles was 0.48 deg, which is less than half of that reported in earlier comparable studies (Hubel & Wiesel, 1962; Creutzfeldt et al., 1974; Albus, 1975*a*) done at about the same visual field eccentricity as here (5–10 deg). As expected, we found that receptive-field scatter increased with receptive-field size, but the group scatter ($4\sigma = 1.94$ deg) was about half of the mean group receptive-field size of 3.80 deg. In only two of the 53 groups of three or more cells recorded was scatter more than the mean group receptive-field size. Creutzfeldt et al.'s (1974) similar measure of scatter was 3.64 deg (4σ) with an average receptive-field size of 2.9 deg (1.26:1). Albus (1975*a*) also reported a range of scatter measures (4σ) from 1.2 deg to 6.4 deg with average receptive-field sizes ranging from 0.7 deg to 2.6 deg. We believe our measures were lower for at least two reasons. First, our measurements were based on groups of cells recorded simultaneously, not sequentially. When Creutzfeldt et al. (1974) analyzed 20 pairs of simultaneously recorded cells, the mean difference between their response peaks was 0.9 deg $\pm$ 0.56 deg, which is very near the average difference between receptive-field center positions that we obtained (0.82 deg $\pm$ 0.59 deg). Second, we sampled both the dark (OFF) and light bar (ON) regions of the receptive field and fit the response profiles with either Gaussian or Gabor functions. The minimum response field method of receptive-field plotting (Barlow et al., 1967) results in larger estimates of scatter (Creutzfeldt et al., 1974) and smaller receptive-field sizes (Dow et al., 1981). Thus, scatter was more likely than not to have been overestimated and receptive-field size underestimated, in these studies. It is possible that scatter in the macaque monkey has also been overestimated, given that hand plotting and sequential recording were used by Hubel and Wiesel (1974*b*) in their study of receptive-field position scatter.

We found no difference between the absolute amounts of scatter in the horizontal and vertical directions, or between ipsilateral and contralateral eyes. Some early studies reported greater amounts of horizontal than vertical scatter (Blakemore, 1969; Blakemore & Pettigrew, 1970) and greater ipsilateral than contralateral scatter (Blakemore & Pettigrew, 1970). However, other studies have failed to find these differences (Nikara et al., 1968; Albus, 1975*a*; von der Heydt et al., 1978; Bishop, 1979). A greater amount of horizontal scatter is a theoretically attractive possibility because of the likelihood that it might underlie a mechanism in which depth information was obtained from horizontal disparities. However, because vertical disparities can also provide depth information (Mayhew & Longuet-Higgins, 1982; Bishop & Pettigrew, 1986; Bishop, 1989) one might, on this basis, expect some degree of vertical receptive-field position scatter as well.

Bishop (1979) suggested that receptive-field position scatter might underlie disparity detection. He pointed out that if scatter in the two eyes was independent, then the average disparity would be given by the quadratic sum of the two monocular scatters. Our findings suggest however that scatter in the two eyes is not independent, since horizontal, as well as vertical, receptive-field position deviations from the local group mean are correlated in the two eyes. Nevertheless, a significant amount of residual variation in inter-ocular receptive-field position difference exists, and although some of this can probably be attributed to measurement error, and to anatomical scatter, probably not all of it can, and the remaining inter-ocular scatter may make a significant contribution to dispar-

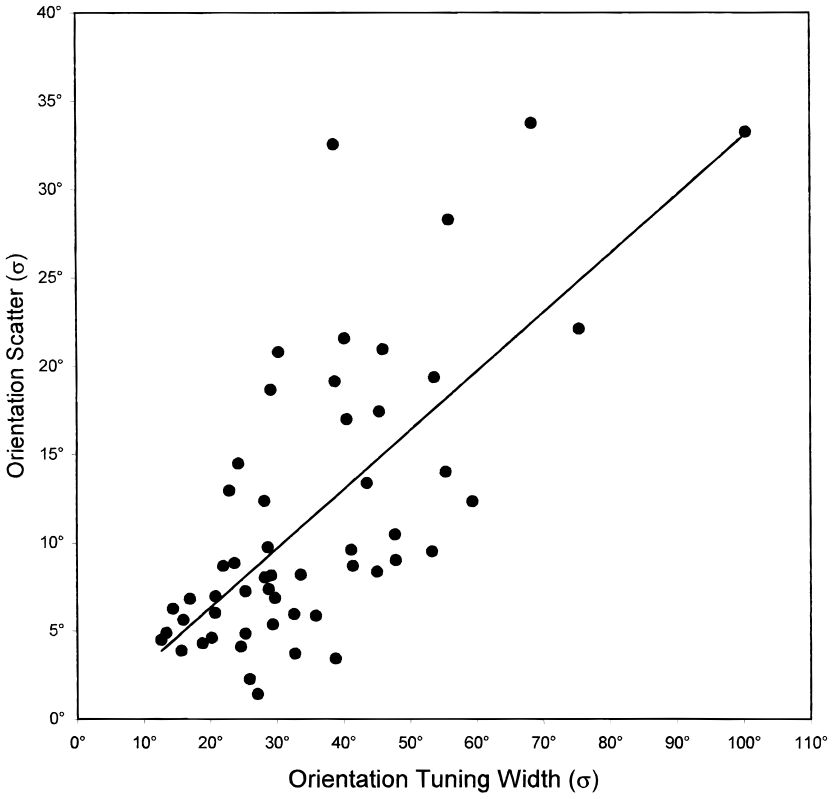

Fig. 9. Scatter plot showing, for all ensembles of three or more cells, orientation tuning width (*x* axis) *versus* orientation scatter (*y* axis): there was a strong positive correlation between the average width of orientation tuning and orientation scatter within ensembles.

ity detection. In addition, by expressing deviations relative to the group mean in each eye, we have implicitly assumed that the group means are the same. However, there will be random errors in our estimates of these means, which will add to the estimates of actual disparity. Nor can we rule out the possibility that systematic differences in group means exist, that is, that the retinotopic maps in the two eyes are systematically misaligned, possibly in a way that leads to an ordered map of disparity.

Our results suggest that randomness in the cortical representation makes a relatively slight contribution to the size of the cortical point image (the set of neurons whose receptive fields cover a particular point in visual space). Assuming a cortical magnification factor of 2 deg/mm, an average receptive-field diameter ($= 4\sigma_{\text{r.f.}}$) of 3.8 deg and no scatter at all, the point image will have a diameter = 1.9 mm. The addition of random Gaussian scatter with $\sigma_{\text{scat}} = 0.48$ deg to this (i.e. convolving the Gaussian receptive-field profile with the Gaussian scatter, which causes $\sigma_{\text{r.f.}}$ and σ_{scat} to add quadratically) yields an only slightly increased point image size $= 4 \times (0.95^2 + 0.48^2)^{1/2} \div 2$ deg/mm = 2.13 mm in diameter. If point image is defined instead in terms of receptive-field centers (i.e. to include only those neurons maximally activated by a stimulus), its diameter $= 4 \times 0.48$ deg $\div 2$ deg/mm = 0.96 mm is smaller than the repeat period of the orientation columns. This raises the possibility that some combinations of orientation and position in visual space may fail to maximally activate cortical neurons, although neurons may be activated submaximally *via* flanking receptive-field regions.

Orientation scatter

The average difference in orientation preference between two neighboring cortical cells in area 17 was about 15 deg, and the mean group scatter across all 53 sites of three or more cells was about ±13.6 deg. These estimates are similar to those found in previous studies in the cat (Albus, 1975*b*; Lee et al., 1977; Murphy & Sillito, 1986) including a study using tetrodes (Maldonado & Gray, 1996; Maldonado et al., 1997). Although these authors suggested that this scatter represents physiological disorder at the cellular level in the orientation map, it seems possible that much, or possibly even all, of the apparent disorder might be caused by scatter in the anatomical positions of recorded cells relative to the electrode. Maldonado and Gray (1996, p. 512) considered this possibility, but in the context of a linear orientation map with parallel iso-orientation domains. We have found that the presence of orientation pinwheels in the map significantly increases the impact of anatomical scatter on measured orientation scatter. Our conclusion about the impact of anatomical scatter however depends most strongly on the assumptions we have made about the seeing distance of our tetrodes. These assumptions are difficult to evaluate, and are likely to depend on several factors including the shape and diameter of the tetrode, the impedance of the individual electrodes, and the angle of the tetrode tips relative to cortical columns. If the seeing distance is less than we have assumed, there could still be a significant amount of physiological scatter. For example, since standard deviations add quadratically, an overall scatter of ±13.6 deg might be explained by separate and roughly equal anatomical and physiological components of about ± 9.6 deg. The explanation of the finding that orientation scatter is correlated in the two eyes is similarly uncertain: the correlation is consistent with an anatomical source of scatter, but real inter-ocular scatter of a few degrees cannot be ruled out either.

Other observations suggest that anatomical scatter has a significant impact on our measurements, although they do not allow an exact evaluation of its magnitude. First, a small but significant

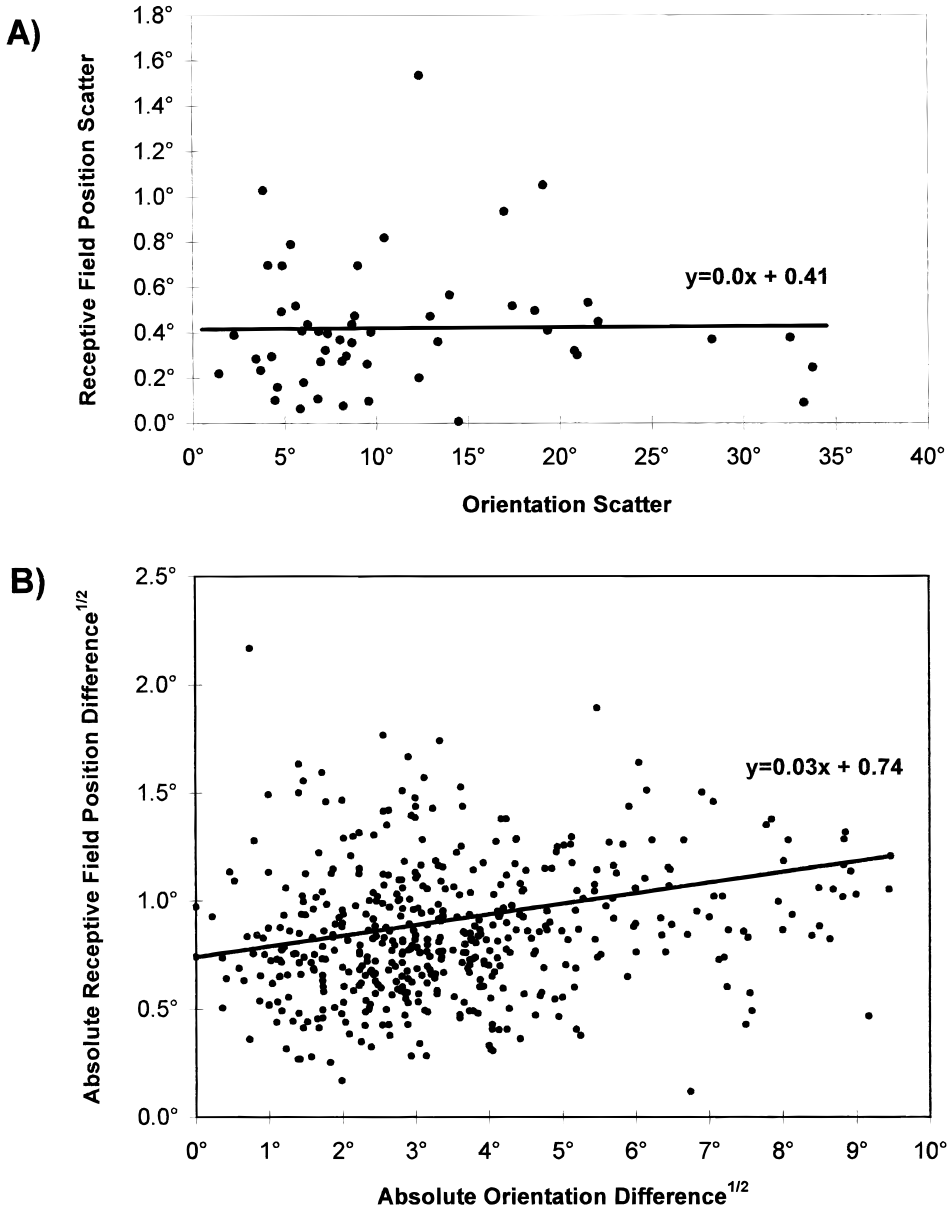

Fig. 10. (A) Scatter plot showing, for all ensembles of three or more cells, orientation scatter (x axis) versus receptive-field scatter (y axis): there was no indication that those groups of cells with large variations in orientation preference showed similar large variations in receptive-field scatter. (B) Scatter plot showing, for all simultaneously recorded cell pairs, the difference in receptive-field center positions (y axis) *versus* the difference in preferred orientations (x axis).

correlation was found between cell pair orientation, and receptive-field position, differences (Fig. 10). Second, we found a positive correlation between cell pair receptive-field position differences, and distances between the cells in a spike parameter space. Distances in this space are likely to correlate with cortical distance, and therefore also with receptive-field position. However, we found no such correlation between cortical distance and cell pair orientation difference. Thus, it is tempting to explain the first result by assuming that cell pairs showing large differences in preferred orientation are, on average, farther apart than those with similar preferred orientations, and that such pairs will, on average, have receptive fields that are also farther apart; but, we must reject this explanation given our second finding. Instead, we offer two alternative explanations: (1) the relationship between orientation and receptive-field cell pair position differences was simply a statistical accident; after all, the correlations between receptive field and orientation group scatter ($r = 0.01$, $N = 53$), and between receptive field and orientation individual deviations ($r = 0.07$, $N = 256$) were not statistically significant. Or (2), the relationship reflected a real, intrinsic, and functionally important property of neurons which has nothing to do with anatomical scatter. However, without additional data, we cannot favor one explanation over the other.

Unlike Maldonado et al. (1997), we did not find a significant correlation between depth of recording and orientation scatter. However, they reported that scatter varied with depth only for those penetrations within linear zones, distant from singularities, and the strength of the correlation appeared weak (no strength was given). Earlier studies report little or no evidence that orientation

scatter varies with cortical depth (e.g. Hubel & Wiesel, 1963; Lee et al., 1977; Murphy & Sillito, 1986).

We found a strong correlation ($r = 0.70$) between orientation scatter and orientation tuning or bandwidth (Fig. 9): that is, regions of cortex in which measured orientation scatter was large had relatively broad orientation tuning and regions in which scatter was small had relatively narrow tuning. This result stands in contrast to the findings of Maldonado et al. (1997) who reported that orientation tuning of cells in, or near, orientation singularities was as sharp as that of cells in other locations. One possible explanation for our finding is that it is an artifact of measurement error, and that errors in the estimates of preferred orientation (and hence apparent scatter) increase when orientation tuning curves are broad and decrease when the curves are narrow. However, estimates of the accuracy of our curve-fitting procedures for a few cells, and comparisons with the simulations reported by Swindale (1998), suggest that our measurement errors are too small to account for more than a small proportion of the observed scatter, even in broadly tuned cells. Two remaining explanations are that (1) Maldonado et al. (1997) made errors in locating their electrodes relative to singularities (which were defined on the basis of prior optical recording) and (2) that there are regions within which orientation scatter and/or gradient is large, and tuning widths are broad, but these regions do not coincide precisely with the orientation singularities (Swindale, 1982).

Relationship between orientation and retinotopic maps

Das and Gilbert (1997) have reported finding, in area 17 of the cat, regions in which receptive-field positions shift relatively rapidly with cortical position. These regions correlate spatially with the orientation singularities, and they found that, in general, spatial rates of change of both properties were strongly and positively correlated. Our findings give little hint of such a correlation, although they do not explicitly contradict these results. For example, we found no correlation between receptive-field position scatter and orientation scatter across ensembles (Fig. 10A), which might have been expected if the measures of scatter are at least partially determined by local spatial gradients in the two maps. In four cats, we recorded eight sites where the standard deviation of orientation preferences exceeded 20 deg, yet the mean group scatter in receptive-field positions across these sites was 0.41 deg, which is even lower than the overall mean group scatter (0.48 deg). Although we occasionally found pairs of neurons with very dissimilar preferred orientations (indicating that the cells might have been close to a singularity), the receptive-field position differences of these pairs seemed only slightly larger than those of other cell pairs, and certainly no differences as large as those reported by Das and Gilbert were found (Fig. 10B). However, it is possible that none of our recording sites was close to a singularity or other region of rapid orientation gradient. Also, although Fig. 10 shows a weak positive correlation between cell pair orientation and receptive-field position differences, these differences cannot be interpreted as gradient measures without knowing the anatomical locations of the cells in each pair. Given random variation in the distances between cells, we would expect a positive correlation, even if both orientation and topographic maps were completely uniform, with no gradient variations.

There are three other potentially relevant differences between our methods and Das and Gilbert's. First, our receptive-field maps were single unit, not multiunit. Recording from multiple units will necessarily increase receptive-field size and decrease receptive-field scatter, and increase any correlation between receptive field and orientation scatter (although decrease the power). Second, their receptive-field scatter measure was normalized to receptive-field size, so the correlation with orientation scatter may have been between receptive-field size and orientation scatter. However, we found no indication that receptive-field size varied with orientation scatter in our data. Third, the distances over which receptive fields were compared in their study were far greater than the local distances between our cell pairs. However, given their results from cell pairs less than 200 μm apart, we still should have seen some large receptive-field cell pair differences.

Effects of stimulus velocity on field sizes

It is possible that the use of moving bars could have led to an overestimation of receptive-field size and scatter. To take an extreme case, if two cells with identical receptive-field positions responded only to opposite directions of motion and had a firing latency of 50 ms, and were stimulated by a bar moving at 6 deg/s, their measured receptive-field center positions would differ by 0.6 deg. However, the actual error in our measurements due to firing latency is likely to be much less than this. First, in the majority of experiments the bar velocity was less than 6 deg/s (2 or 3 deg/s was typical). Second, if the orientation and direction preferences of the receptive fields are similar, then what is important is not the absolute latency, but latency variation between cells. These variations are likely to be about ± 10 ms or even less (see Swindale & Mitchell, 1994). If we assume a latency scatter of ± 10 ms and a bar velocity of 3 deg/s, then the resulting positional scatter would be ± 0.03 deg, which is much less than what we actually measured. Orientation scatter will add only a small amount to this: if the average scatter is around ± 13 deg and each cell has an absolute latency of 50 ms and the stimulus moves at 6 deg/s, the contribution to scatter is about $0.05 \times 6.0 \times \sin(13 \text{ deg}) = \pm 0.067$ deg. Finally, if there are additional measurement errors, these will have inflated our estimates of scatter and this means that real physiological scatter will necessarily be even smaller than we have estimated.

Conclusions

Our results suggest that, on a cellular level, the retinotopic and orientation maps in cat area 17 are less random and more highly organized than was previously thought. Expressed in terms of the same underlying Gaussian width parameter σ, scatter in receptive-field center positions is about half of receptive-field size, on average, and is likely to make a relatively small contribution to the size of the cortical point image. Scatter in the map of preferred orientation is likely to be less than ± 13 deg, and might even be substantially less than this. Scatter is not independent in the two eyes: deviations from the local mean for both preferred orientation and receptive-field position are correlated in the two eyes although a significant amount of residual inter-ocular orientation and receptive-field position scatter exists. Regions of cortex showing larger amounts of orientation scatter appear to have broader orientation tuning. Receptive-field position scatter did not correlate with orientation scatter.

Acknowledgments

We thank Virginia Booth and Dichen Zhao for their helpful assistance. This research was supported by MRC of Canada (MT-12848) and by NSERC (OGP0178702).

References

Albus, K. (1975*a*). A quantitative study of the projection area of the central and the paracentral visual field in area 17 of the cat I. The precision of the topography. *Experimental Brain Research* **24**, 159–179.

Albus, K. (1975*b*). A quantitative study of the projection area of the central and the paracentral visual field in area 17 of the cat II. The spatial organization of the orientation domain. *Experimental Brain Research* **24**, 159–179.

Anzai, A., Ohzawa, I. & Freeman, R.D. (1997). Neural mechanisms underlying binocular fusion and stereopsis: Position *vs.* phase. *Proceedings of the National Academy of Sciences of the U.S.A.* **94**, 5438–5443.

Barlow, H.B., Blakemore, C. & Pettigrew, J.D. (1967). The neural mechanism of binocular depth perception. *Journal of Physiology* (London) **193**, 327–342.

Barlow, H.B., Blakemore, C. & Van Sluyters, R.C. (1974). Measurement of residual eye movements during the analysis of disparity of receptive fields of visual neurons. *Journal of Physiology* (London) **242**, 38–39.

Barlow, R.J. (1989). *Statistics: A Guide to the Use of Statistical Methods in the Physical Sciences*. New York: John Wiley & Sons.

Batschelet, E. (1981). *Circular Statistics in Biology*. London: Academic Press.

Bishop, P.O. (1979). Stereopsis and the random element in the organization of the striate cortex. *Proceedings of the Royal Society B* (London) **204**, 415–434.

Bishop, P.O. (1989). Vertical disparity, egocentric distance and stereoscopic depth constancy: A new interpretation. *Proceedings of the Royal Society B* (London) **237**, 445–469.

Bishop, P.O., Henry, G.H. & Smith, C.J. (1971). Binocular interaction fields of single units in the cat striate cortex. *Journal of Physiology* (London) **216**, 39–68.

Bishop, P.O. & Pettigrew, J.D. (1986). Neural mechanisms of binocular vision. *Vision Research* **26**, 1587–1600.

Blakemore, C. (1969). Binocular depth discrimination and the nasotemporal division. *Journal of Physiology* (London) **205**, 471–407.

Blakemore, C., Fiorentini, A. & Maffei, L. (1972). A second neural mechanism of binocular depth perception. *Journal of Physiology* (London) **226**, 725–740.

Blakemore, C. & Pettigrew, J.D. (1970). Eye dominance in the visual cortex. *Nature* **225**, 426–429.

Blasdel, G.G. & Salama, G. (1986). Voltage sensitive dyes reveal a modular organization in monkey striate cortex. *Nature* **321**, 579–585.

Bonhoeffer, T. & Grinvald, A. (1991). Iso-orientation domains in cat visual cortex are arranged in pinwheel-like patterns. *Nature* **353,** 429–431.

Chow, K.L. & Lindsley, D.F. (1968). Influence of residual eye movements in single-unit studies of the visual system. *Brain Research* **8**, 385–388.

Cooper, M.L. & Pettigrew, J.D. (1979). A neurophysiological determination of the vertical horopter in the cat and owl. *Journal of Comparative Neurology* **184**, 1–26.

Creutzfeldt, O., Innocenti, G.M. & Brooks, D. (1974). Vertical organization in the visual cortex (area 17) in the cat. *Experimental Brain Research* **21**, 315–336.

Cynader, M.S., Swindale, N.V. & Matsubara, J.A. (1987). Functional topography in cat area 18. *Journal of Neuroscience* **7**, 1401–1413.

Daniel, P.M. & Whitteridge, D. (1961). The representation of the visual field on the cerebral cortex in monkeys. *Journal of Physiology* (London) **159**, 203–221.

Das, A. & Gilbert, C.D. (1997). Distortions of visuotopic map match orientation singularities in primary visual cortex. *Nature* **387**, 594–598.

DeAngelis, G.C., Anzai A., Ohzawa, I. & Freeman R.D. (1995). Receptive field structure in the visual cortex: Does selective stimulation induce plasticity? *Proceedings of the National Academy of Sciences of the U.S.A.* **92**, 9682–9686.

Diao, Y.-C., Jia, W.-G., Swindale, N.V. & Cynader, M.S. (1990). Functional organization of the cortical 17/18 border region in the cat. *Experimental Brain Research* **79**, 271–282.

Dow, B.M., Snyder, A.Z., Vautin, R.G. & Bauer, R. (1981). Magnification factor and receptive field size in foveal striate cortex of the monkey. *Experimental Brain Research* **44**, 213–228.

Drake, K.L., Wise, K.D., Farraye, J., Anderson, D.J. & BeMent, S.L. (1988). Performance of planar multisite microprobes in recording extracellular single-unit intracortical activity. *IEEE Transactions Biomedical Engineering* **35**, 719–732.

Fisher, N.I. (1995). *Statistical Analysis of Circular Data*. New York: Cambridge University Press.

Gray, C.M., Maldonado, P.E., Wilson, M. & McNaughton, B. (1995). Tetrodes markedly improve the reliability and yield of multiple single-unit isolation from multi-unit recordings in cat striate cortex. *Journal of Neuroscience Methods* **63**, 43–54.

Hetherington, P.A., Zakarauskas, P. & Swindale, N.V. (1996). Rotated hyper-ellipses improve multi-unit spike separation. *Society for Neuroscience Abstracts* **22**, 1608.

Heydt, R. von der, Adorjani, C., Hänny, P. & Baumgartner, G. (1978). Disparity sensitivity and receptive field incongruity of units in the cat striate cortex. *Experimental Brain Research* **31**, 523–545.

Hubel, D.H. & Wiesel, T.N. (1962). Receptive fields, binocular interaction and functional architecture in the cat's visual cortex. *Journal of Physiology* (London) **160**, 106–154.

Hubel, D.H. & Wiesel, T.N. (1963). Shape and arrangement of columns in cat's striate cortex. *Journal of Physiology* (London) **165**, 559–568.

Hubel, D.H. & Wiesel, T.N. (1968). Receptive fields and functional architecture of monkey striate cortex. *Journal of Physiology* (London) **195**, 215–243.

Hubel, D.H. & Wiesel, T.N. (1974*a*). Sequence regularity and geometry of orientation columns in monkey striate cortex. *Journal of Comparative Neurology* **158**, 267–294.

Hubel, D.H. & Wiesel, T.N. (1974*b*). Uniformity of monkey striate cortex: A parallel relationship between field size, scatter, and magnification factor. *Journal of Comparative Neurology* **158**, 295–306.

Humphrey, D.R., Corrie, W.S. & Rietz, R.R. (1978). Properties of the pyramidal tract neuron system within the precentral wrist and hand area of primate motor cortex. *Journal of Physiology* (Paris), **74**, 215–226.

Jones, J.P. & Palmer, L.A. (1987). An evaluation of the two-dimensional Gabor filter model of simple receptive fields in cat striate cortex. *Journal of Neurophysiology* **58**, 1233–1258.

Lee, B.B., Albus, K., Heggelund, P., Hulme, M.J. & Creutzfeldt, O.D. (1977). The depth discrimination of optimal stimulus orientations for neurones in cat area 17. *Experimental Brain Research* **27,** 301–314.

Löwel, S., Freeman, B. & Singer, W. (1987). Topographic organization of the orientation column system in large flat-mounts of the cat visual cortex: A 2-deoxyglucose study. *Journal of Comparative Neurology* **155**, 401–415.

Maldonado, P.E., Gödecke, I., Gray, C.M. & Bonhoeffer, T. (1997). Orientation selectivity in pinwheel centers in cat striate cortex. *Science* **276**, 1551–1555.

Maldonado, P.E. & Gray, C.M. (1996). Heterogeneity in local distributions of orientation-selective neurons in the cat primary visual cortex. *Visual Neuroscience* **13**, 509–516.

Marcelja, S. (1980). Mathematical description of the responses of simple cortical cells. *Journal of the Optical Society of America* **70**, 1297–1300.

Mayhew, J.E.W. & Longuet-Higgins, H.C. (1982). A computation model of binocular depth perception. *Nature* **297**, 376–378.

Mountcastle, V.B., Davies, P.W. & Berman, A.L. (1957). Response properties of cat's somatosensory cortex to peripheral stimuli. *Journal of Neurophysiology* **29**, 374–407.

Murphy, P.C. & Sillito, A.M. (1986). Continuity of orientation columns between superficial and deep laminae of the cat primary visual cortex. *Journal of Physiology* (London) **381**, 95–110.

Nelder, J.A. & Mead, R. (1965). A simplex method for function minimization. *Computer Journal* **7**, 308–313.

Nelson, J.I., Kato, H. & Bishop, P.O. (1977). Discrimination of orientation and position disparities by binocularly activated neurons in cat striate cortex. *Journal of Neurophysiology* **40**, 260–283.

Nikara, T., Bishop, P.O. & Pettigrew, J.D. (1968). Analysis of retinal correspondence by studying receptive fields of binocular single units in the cat striate cortex. *Experimental Brain Research* **6**, 353–372.

Rodieck, R.W., Pettigrew, J.D., Bishop, P.O. & Nikara, T. (1967). Residual eye movements in receptive-field studies of paralyzed cats. *Vision Research* **7**, 107–110.

Swindale, N.V. (1982). A model for the formation of orientation columns. *Proceedings of the Royal Society B* (London) **215**, 211–230.

Swindale, N.V. (1996). The development of topography in the visual cortex: A review of models. *Network: Computation in Neural Systems* **7**, 161–247.

SWINDALE, N.V. (1998). Orientation tuning curves: Empirical description and estimation of parameters. *Biological Cybernetics* **78**, 45–56.

SWINDALE, N.V. & MITCHELL, D.E. (1994). Comparison of receptive field properties of neurons in area 17 of normal and bilaterally amblyopic cats. *Experimental Brain Research* **99**, 399–410.

SWINDALE, N.V., CYNADER, M.S. & MATSUBARA, J. (1990). Cortical cartography: A two-dimensional view. In *Computational Neuroscience*, ed. SCHWARTZ, E., pp. 232–341. Cambridge, Massachusetts: MIT Press.

TABACHNICK, B.G. & FIDELL, L.S. (1989). *Using Multivariate Statistics* (2nd edition), pp. 83–85. Harper Collins Publishers, Inc., New York.

TUSA, R.J., PALMER, L.A. & ROSENQUIST, A.C. (1978). The retinotopic organization of area 17 (striate cortex) in the cat. *Journal of Comparative Neurology* **177**, 213–236.

WOLF, F. & GEISEL, T. (1998). Spontaneous pinwheel annihilation during visual development. *Nature* **395**, 73–78.